Macromolecules

ARTICLE

pubs.acs.org/Macromolecules

# 2D-Infrared Thermography Monitoring of Ultrasound-Assisted Polymerization of Water-Soluble Monomer in a Gel Process

Julien Rigolini,[†] Florine Bombled,[†] Francis Ehrenfeld,[†] Kamal El Omari,[‡] Yves Le Guer,[‡] and Bruno Grassl*[,†]

[†]Institut Pluridisciplinaire de Recherche Environnement et Matériaux (IPREM UMR 5254), Equipe de Physique et Chimie des Polymères (EPCP), Université de Pau et des Pays de l'Adour (UPPA), Hélioparc, Avenue P. Angot, 64000 Pau, France

[‡]Laboratoire des Sciences de l'Ingénieur Appliquées à la Mécanique et au Génie Electrique (SIAME), Fédération IPRA, Université de Pau et des Pays de l'Adour (UPPA), Bat. D'Alembert, rue Jules Ferry, BP 7511, 64075 Pau Cedex, France

Supporting Information

**ABSTRACT:** This paper describes a process based on the ultrasound-assisted polymerization of a water-soluble monomer at a high concentration, which is known as a gel polymerization process. Polymerization is triggered by the ultrasound-assisted decomposition of the initiating species. This highly exothermic polymerization reaction can sustain a localized reaction front that propagates throughout an unstirred medium, as in frontal polymerization. Evidence for the controlled nature of thermal propagation alongside a gel process is presented by online 2D-infrared (IR) thermography monitoring. In addition, the effects of thermal propagation on the molar mass distributions are described. Specifically, the use of ultrasound not only suppresses the so-called "fingering" of frontal polymerization but also avoids any alteration of the molar mass distribution of the polymer.

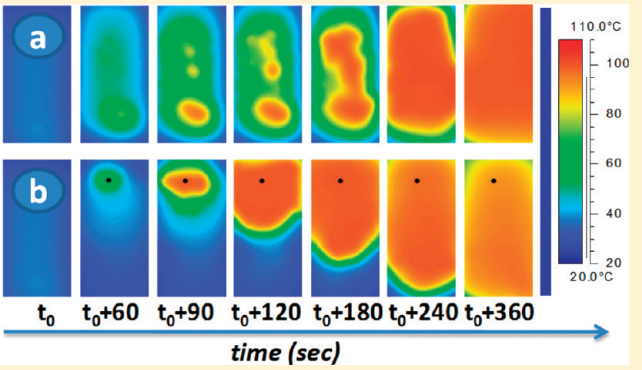


## 1. INTRODUCTION

The synthesis of acrylic polymers as rheology modifiers for water-based systems may be carried out by methods that include gel polymerization, precipitation polymerization, and inverse emulsion polymerization processes. A gel polymerization (GP) process is usually used as a manufacturing method for the production of rheology modifiers based on polyacrylamide for use in tertiary oil recovery, drilling fluids, hydraulic fracturing, and drag reduction. This method involves preparing a solution of acrylamide monomer or a mixture of comonomers in water at a high concentration (20−50 wt %). This monomer concentration is influenced by the calculated exothermic reaction of the monomer mixture, the temperature at which the polymerization is initiated (5−30 °C), the heat capacity of the continuous phase, and any heat losses or deliberate cooling effects applied during the course of the reaction. At the end of the polymerization process, the water-thin monomer solution is converted into a tough gel with a rubbery consistency. To supply the product to the end user in an easy-to-handle and cost-effective manner, it is common practice to remove the water from the polymer gel. This is achieved more easily if the gel is cut or processed into small particles before being subjected to dehydration, often using a fluid bed drier. This batch-based process has been carried out on an industrial scale for over 30 years and is often favored for achieving the highest molecular weight grades in anionic, nonionic and cationic chemical types.[1,2] Recently, our group used GP for associative polymer synthesis[3] and the controlled radical polymerization of acrylamide via nitroxide-mediated polymerization; the latter being implemented both with a classic method[4] and with a microwave-assisted process.[5,6]

In the context of GP, this paper reports for the first time the ultrasound-assisted polymerization of a water-soluble polymer via a gel process. The method is based on a frontal polymerization[7−15] method in which a localized exothermic reaction zone is produced due to the coupling of thermal diffusion and the Arrhenius kinetics of the exothermic polymerization. Once polymerization is triggered by the ultrasound-assisted decomposition of the initiating species, this highly exothermic reaction can sustain a localized reaction front that propagates throughout an unstirred medium. Unlike frontal polymerization, GP does not involve a significant difference in the refractive index for the synthesized polymer versus the monomer/initiator mixture, which would make it possible to optically monitor the progression of the front and to determine its velocity through distance versus time plots. Thus, 2D-IR thermography monitoring of the gel process is used as a realistic

**Received:** March 27, 2011
**Revised:** April 22, 2011
**Published:** May 10, 2011

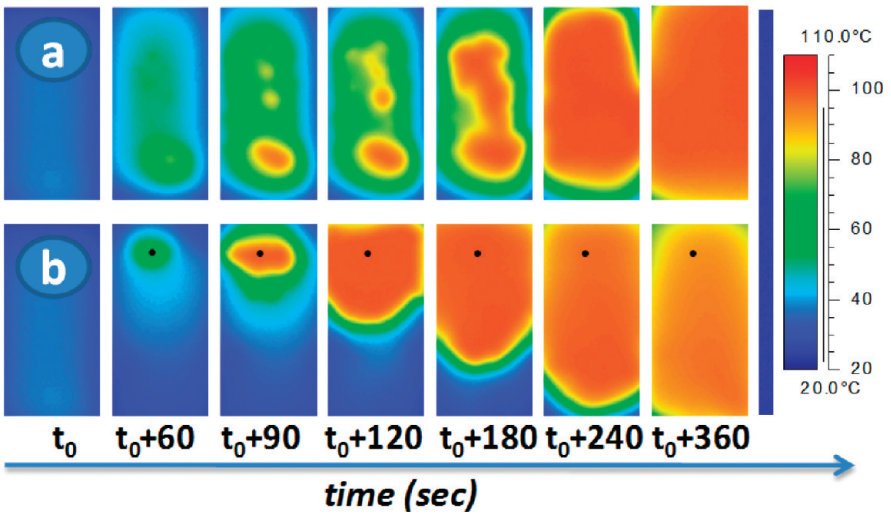


**Figure 1.** Montage of infrared images of a plane reactor (reactor = 300 × 150 × 15 $mm^3$ and frame = 250 × 125 $mm^2$). (a) Top: Nonultrasound-assisted polymerization. (b) Bottom: Ultrasound-assisted polymerization of 35 wt % acrylamide ($t_0$ was taken as an arbitrary time before polymerization). The black point indicates the US probe center position.

approach for frontal polymerization analysis.[16,17] Since the first pioneering work on frontal polymerization in 1972 by Chechilo and Enikolopyan,[18] who studied methyl methacrylate polymerization under adiabatic conditions at high pressures, a great number of studies have been quickly conducted on this versatile and easily implemented methodology for synthesizing a wealth of uniform polymers and polymeric networks with spatially controlled microstructures and morphologies.[7,8,10,19−45] To the best of our knowledge, there has been no prior report on ultrasound as a trigger to synthesize water-soluble polymers in a gel process. In this context, the aims are to monitor frontal polymerization using a recent advanced analytical method, that is, IR thermography, and to evaluate the impact of the gel process on the molar mass distribution of water-soluble polymers.

The issue of the effect of ultrasound on radical polymerization in a gel process is the primary focus of this work. To that end, we chose to carry out ultrasound-assisted polymerizations of acrylamide at a high concentration (35 wt %) in a purely aqueous solution using a conventional hydrosoluble radical initiator (Vazo56). Evidence of the controlled nature of thermal propagation during the gel process is presented using online 2D-infrared thermography monitoring, and the effects of thermal propagation on the molar mass distributions are described.

## 2. EXPERIMENTAL SECTION

**2.1. Materials.** Acrylamide (AM) (purity >99%) was purchased from ABCR, and 2,2-azobis (2-methylpropionamidine) dihydrochloride, denoted by Vazo56, was obtained from Aldrich. All chemical products were used as received. Deionized water, with an electrical conductivity of 18 MΩ.cm at 25 °C, was filtered through a 0.22 $\mu$m Millipore filter prior to use.

**2.2. Polymerization.** Poly(acrylamide) PAM and the corresponding copolymers were prepared by classical radical polymerization initiated with Vazo56. For example, a given amount (350 g) of acrylamide AM was dissolved in 550 mL of Milli-Q water. After a 60 min purified nitrogen purge of the AM solution, 100 mL (0.13 $mol \cdot L^{-1}$) of an aqueous solution of Vazo56 was added to it. The reaction was conducted in a home-built plane reactor for 2D-IR thermography monitoring or in a 500 mL water-jacketed cylindrical reaction vessel equipped with a thermometer, a nitrogen inlet and ultrasound probe.

The home-built plane reactor was composed of two stainless steel plates (300 × 300 $mm^2$ or 150× 300 $mm^2$, thickness =2 mm, depending on the useful volume of the reactor) that were 15 mm apart, fastened with a U-shaped plastic holder and an O-ring gasket to ensure the sealing. All of this was surrounded by an aluminum holder equipped with clamping screws to ensure the turning out of the gel at the end of the reaction (see Figure S1 in the Supporting Information). The thermal conductivity of the stainless steel was 16.2W/mK, and the plates were externally covered with black matte paint to ensure an emissivity of 0.92. Sonication was carried out with a 13 mm diameter probe connected to a sonicator BIOBLOCK *Vibra Cell 72408* (400 W, 20 kHz) used at an amplitude of 10%. The probe was centered in the plane reactor with 50 to 60 mm of immersion. An unmodified FLIR Thermacam SC500, which is an infrared camera (FLIR Systems, Inc.) equipped with thermaCAM researcher software (version 2.33), was used in the experiments. This instrument has a sensitivity of ±0.5 °C with an operating temperature range of −40 to +500 °C. The IR camera was positioned at 90° to the reactor plate and focused on this one, as illustrated in the Supporting Information (Figure S1). Online 2D-IR thermography monitoring was carried out in a black enclosure to protect the reactor plate from external radiation in the infrared range of the electromagnetic spectrum (7.5−13 $\mu$m). At the end of polymerization, some points of the reactive media were sampled for SEC measurements to derive molar masses, distributions and residual monomer content. As the product had the characteristics of a gel, it was cut into cylindrical pellets smaller than 15 mm in diameter with a pastry cutter.

**2.3. Size Exclusion Chromatography Coupled with Multi-angle Light Scattering (SEC−MALS).** The weight-average molar mass ($M_w$), polydispersity ($I_p$), and residual monomer of the polyacrylamide (PAM) samples were determined by size exclusion chromatography (SEC) using a Waters Alliance 2690 chromatograph equipped with four Shodex OHpak columns (SB-807HQ, SB-806HQ, SB-804HQ and SB-802.5HQ) and three online detectors, including a differential refractometer (RI), a UV−visible (UV) photodiode spectrometer, and a DAWN HELEOS II with a 120 mW solid-state laser operating at 658 nm and fitted with a K5 cell. A 0.1 M solution of $NaNO_3$ was used as the eluent at a flow rate of 0.5 mL/min. Samples were prepared by diluting the reaction mixture approximately 350 times in 0.1 M $NaNO_3$ and then filtering with a 0.45 $\mu$m filter (Millipore) after about 2 to 3 days of

stirring. Samples of 50 $\mu$L of these solutions were injected. The weight-average molar mass and polydispersity were obtained from data collected using the ASTRA SEC-software (version 5.3, Wyatt Technology Corp.). The calculation of molar mass was carried out according to the Zimm fit method. The differential molar mass distribution was carried out according to the common form: $x(M) = dW(M)/d[\log(M)]$, where $W(M)$ is the cumulative distribution, i.e., the weight fraction of the sample with a molar mass below $M$. The refractive index increment, $dn/dc$, was determined to be 0.184 ± 0.001 mL/g for polyacrylamide and 0.144 ± 0.001 mL/g for acrylamide.[46]

## 3. RESULTS AND DISCUSSION

**3.1. 2D IR Thermography.** Figure 1 shows the comparison between IR Thermography of spontaneous radical polymerization[47,48] and ultrasound-assisted radical polymerization inside the plane reactor with vertical geometry (300 × 150 × 15 mm$^3$, volume of 450 mL).

In the case without ultrasound, Figure 1a clearly shows the random nature of the initiation step, where the hot spots appear at different places and are then propagated throughout the entire reactor. It may be noted that contrary to the generally accepted idea of a homogeneous initiation step within spontaneous radical polymerization, the initiation and propagation steps take place quickly at different points in the reactor. The high monomer concentration and the strong exothermicity of the polymerization reaction seen at the hot spots show the random and heterogeneous aspects of spontaneous radical polymerization. In contrast to what happens during classical polymerization, the ultrasound-assisted initiation step (Figure 1b) exhibits a hot spot close to the ultrasound probe that is propagated in a homogeneous way along the reactor. This spot appears at a temperature of around 30 °C and sharply increases to around 100 °C, and then it is propagated in all directions.

These observations can be explained by a fast decomposition of the initiator used. Indeed, with the azoinitiator, the production rate of primary radicals is dominated by thermal decomposition, and the initiator efficiency can be defined as the fraction of radicals produced in the homolysis reaction that initiates polymer chains. The disappearance rate of the initiator can be expressed in terms of the initiator half-time ($t_{1/2}$), which is the time it takes for the concentration of the initiator to reach half of its original value. The initiator half-time is temperature dependent, and for Vazo56, it was calculated at a value of 600 min at 56 °C, 9 min at 90 °C and 109 s at 105 °C.[5] After the decomposition of the Vazo56 close to the ultrasound probe, the highly exothermic phase of acrylamide radical propagation increased the temperature sufficiently to initiate polymerization in the neighboring volume and so on throughout the volume of the reactor.

**3.2. Numerical Modeling of Heat Transfer through the Reactor Plate.** The exact localization of the polymerization front using the infrared camera images depends on the transmission of thermal information by thermal conduction through the steel plate. This front is a heat source moving along one side of the plate, and it is necessary to verify that its monitored image on the opposite side of the plate reflects its actual position and is not either farther advanced due to conductivity or delayed due to thermal inertia. Thus, to assess the IR observations, we performed numerical simulations of the heat transfer inside the steel plate. The objective of this simulation was not to reproduce the polymerization phenomenon but to mimic the heat generation and displacement on one side of the plate and to observe the response on the other side.

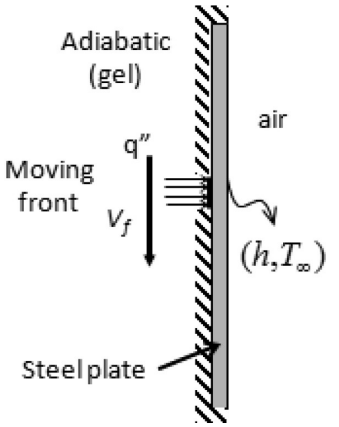


**Figure 2.** Sketch of the 2D model of the plate and its boundary conditions.

For this purpose, we solved the nonsteady state equation for energy conservation, which can be written in integral form as follows.

$$\frac{\partial}{\partial t}\int_V \rho c_p T \, dV = \int_S k\vec{\nabla} T \cdot \vec{n} \, dS$$

Integration was applied to a control volume $V$ surrounded by a surface $S$, which is oriented by the outward unit's normal vector $\vec{n}$. The values $\rho$, $c_p$, and $k$ indicate the density, specific heat and thermal conductivity of the steel plate, respectively. This equation was solved via a finite-volume method using second-order accurate centered differencing for the spatial discretization of the diffusive term and an implicit second-order time scheme. More details on the numerical schemes of the code used can be found in a recent publication.[49] The model used was two-dimensional to represent the thickness of the plate. The computational domain was then a rectangle of dimensions 300 mm × 2 mm (Figure 3). Initially, the plate was at a uniform temperature of 20 °C. The outer side was subject to a convection boundary condition, and the heat transfer coefficient, which takes into account the natural convection to the surrounding air ($T_\infty$ =20 °C), was estimated to be $h$ = 20 W/m$^2$ K. The boundary condition on the inner face was roughly approximated by an adiabatic condition and a moving front of 10 mm in width and to which a heat flux rate $q''$ is applied.

An adiabatic approximation was justified by the following facts.

i Above the front, the plate was in contact with the formed polyacrylamide gel, for which no convection was possible; in addition, it had a low conductivity compared to that of steel.

ii Below the front, there was thermal stratification because heat generation emerged from the top, and therefore, natural convection did not take place.

iii The reactor was symmetric (two parallel steel plates), and thus, there was a zero-flux symmetry condition at 7.5 mm from the plate inside the reactor.

The value of the heat flux rate was estimated by taking into account the reaction heat release of a mass of reactive products contained in a volume of 10 mm × 7.5 mm × 1 m reported for a surface of 10 mm × 1 m throughout the duration of the reaction. To study the effect of the front velocity, two values of its speed $V_f$ were examined. The first corresponded to a front traveling along

300 mm of the plate in 10 min, which yielded $q'' = 3 \times 10^4$ W/m$^2$, and the second speed corresponded to a shorter duration of 1 min, with $q'' = 3 \times 10^5$ W/m$^2$. Experimental observations were between these two extreme values (Figure 2). Different mesh sizes, which were progressively refined, and different time steps were used to obtain independent results according to the grid and time step sizes.

In Figure 3, we plot the temperature profiles at the inner and outer surfaces of the plate at different times of a polymerization; the front is traveling over the plate over a period of 10 min. The curves represent a peak corresponding to the front position moving along the plate with tails of high temperatures to the left and low temperatures (roughly equal to the initial temperature) to the right; below the front, the plate is not affected by the reaction. The inner and outer profiles are superimposed, which indicates that the thermal information on both sides is the same. We also observe a perfect coincidence between the temperature distribution and the peak position in the case of the higher front speed (not shown here), except for a difference in temperature of a few degrees located at the peak. Given these findings, we can estimate that the observations made at the outer surface of the steel plate provide a good indication of the inside of the reactor.

**3.3. Spatiotemporal Frame for Thermal Propagation.** Figure 4a shows a thermal analysis of the front propagation in the form of a 3D plot. The time scale was set arbitrarily to zero at the initiation of camera recording. The depth scale represents the height of the frames in Figure 1 (250 mm) for which the temperature is monitored along the vertical axis of the ultrasound probe. The polymerization initiated at $t = 23.2$ min at the tip of the ultrasound probe; at the probe, the temperature of the medium gradually increased from 23 to 40 °C and then sharply increased to 103 °C in less than 2 min. This increase in temperature propagated the polymerization process throughout the entire reactor. The thermal front propagation was well-defined in line with the ultrasound probe . It began quickly on the level of the probe and then appeared to propagate steadily along the reactor.

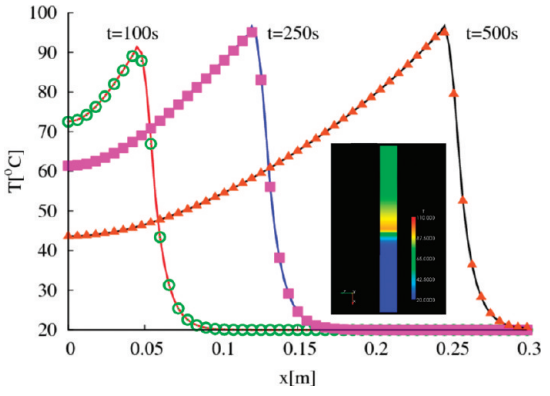


**Figure 3.** Numerical results: temperature profiles along the steel plate at different times. Key: solid lines, inner surface; symbols, outer surface. Inset: temperature distribution at the outer surface ($t = 30$ s).

Figure 4b shows the spatiotemporal frame of thermal propagation. We found that the behavior described above was linear (see the dashed line in Figure 4b), with a thermal front propagation rate estimated at 45 mm/min under our experimental conditions, i.e., 35 wt % of acrylamide and 0.35 wt % of the initiator.

**3.4. Frontal Polymerization Effects on the Molar Masses.** Figure 5 shows an example of temperature monitoring on a reactor with a square geometry (dimension 300 × 300 mm$^2$, volume 1.3 L). The ultrasound probe was plunged into the middle of the reactor at a depth of 60 mm, which is the level at which the hot spot was visualized in frame no. 1 (Figure 5).

In the part of the reactor above the probe that was not insulated and was in contact with the ambient air, the temperature rise was perturbed by the probe. The circular hot spot was rapidly distorted and propagated downward. Alternatively, below the probe, we observed the thermal front propagation described previously.

The thermal front was propagated uniformly in the vertical direction below the ultrasound probe at a rate of 45 mm/min, as in the geometry for the previous reactor. Along the axes at 45° and 90° from the vertical direction, thermal front propagation initially followed the same profile rate, but then it was also disturbed by the top insulated zone of the reactor and the metallic support of the ultrasound probe; as such, the thermal front propagation rate decreased by factors of approximately 2.4 and 3.1, respectively for the axes at 45° and 90° from the vertical direction. However, in a few minutes, polymerization spread throughout the reactor.

It seems that the front dynamics correspond to a planar front propagating through the unreacted polymer solution. We can

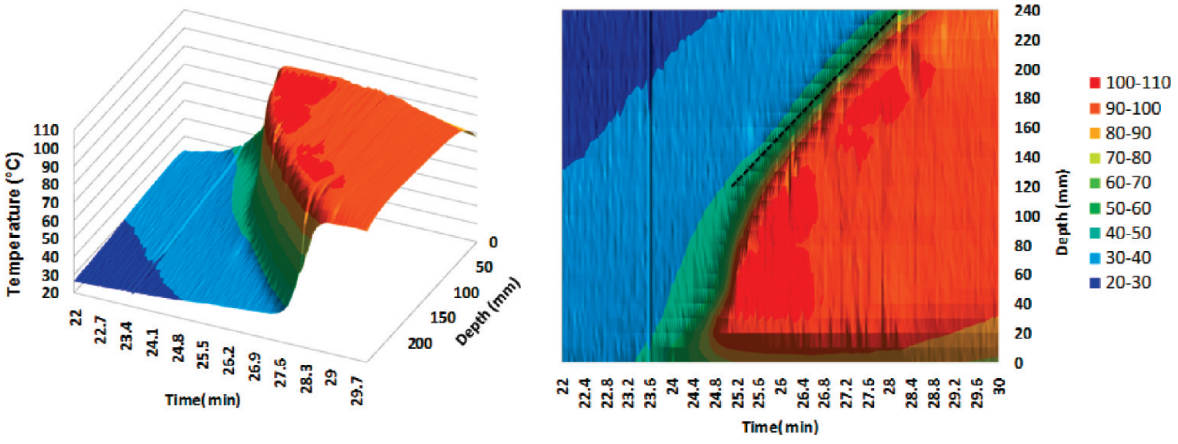


**Figure 4.** (a) A 3D temperature plot; (b) spatiotemporal temperature frame in line with the ultrasound probe (depth = 50 mm) in the plate reactor (300 × 150 × 15 mm$^3$) for acrylamide polymerization (35 wt %).


dx.doi.org/10.1021/ma200706j |*Macromolecules* 2011, 44, 4462–4469

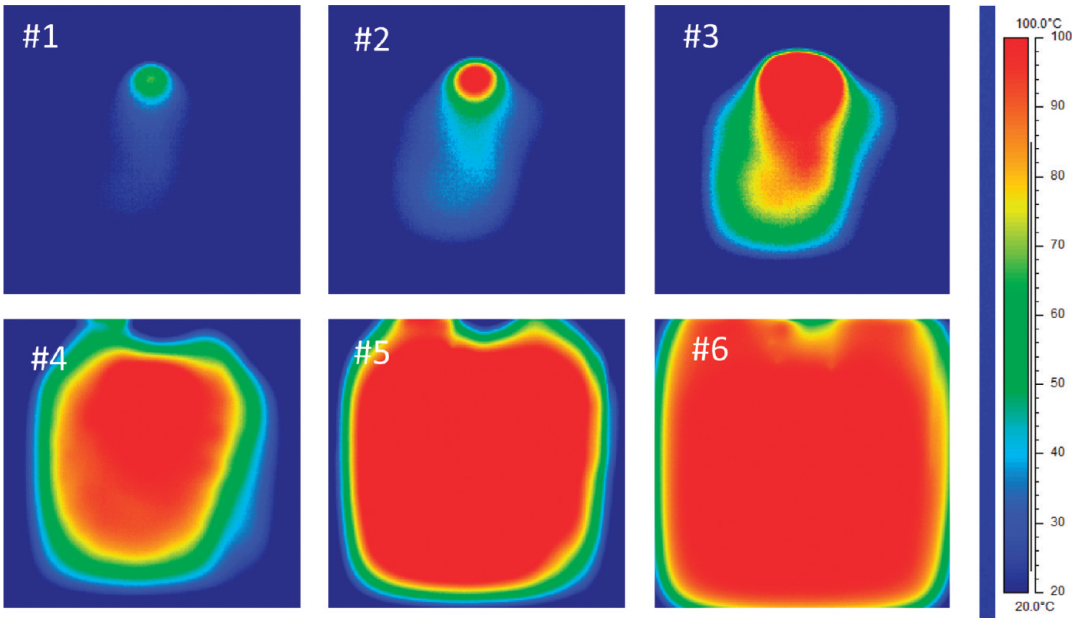


**Figure 5.** Montage of infrared temperature images of a plate reactor (300 × 300 × 15 mm$^3$; frame, 250 × 250 mm). Frame numbers correspond to the following times in seconds: $t_0$+10 (no. 1), 40 (no. 2), 170 (no. 3), 290 (no. 4), 320 (no. 5), and 380 (no. 6) ($t_0$ was taken as an arbitrary time before polymerization).

evaluate a nondimensional parameter, that is, the Zeldovitch number, to estimate the threshold between stable and unstable propagation modes predicted by instability theory.[50−53]

$$Z = \frac{E_a}{RT_{max}}\left(1 - \frac{T_i}{T_{max}}\right)$$

Note that $E_a$ is the activation energy of the acrylamide polymerization (101 KJ mol$^{-1}$);[54] $T_i$ is the initial temperature of the polymer solution; $R$ is the Boltzmann gas constant; and $T_{max}$ is the maximum temperature encountered during thermal front propagation.

Given our experimental conditions and results ($T_i$ = 20−30 °C and $T_{max} \approx$ 100 °C), we derived a Zeldovitch number of approximately 7. The instability theory (under certain assumptions not given here) predicts that when $Z < 8.4$, a planar reaction front propagates at a constant velocity in the reactor. Thus, a steady and stable mode can be observed. Above this threshold value, unstable propagating modes can develop, such as a spinning front.[52,53] Pojman et al.[51] have also shown that unstable modes can be triggered by the shape of the reactor. These considerations, in combination with the fact that the geometric aspect ratio of our reactor is large at 300/15, suggest that a planar front propagation mode has a greater chance of developing in our experiments.

In addition, the homogeneity of the observed thermal front polymerization was compared with the homogeneity of molar mass distributions along the reactor. For this purpose, a sampling was conducted on the final gel-like product once the reactor temperature returned to room temperature. This sampling was carried out using a 9 × 5 matrix form, i.e., a rectangular area delimited by 9 lines and 5 columns (see Figure 6). Each cut-out sample was a cylindrical pellet with a diameter smaller than 15 mm, which was diluted in Milli-Q water for analysis by SEC to obtain the molar mass distributions and the residual monomer content.

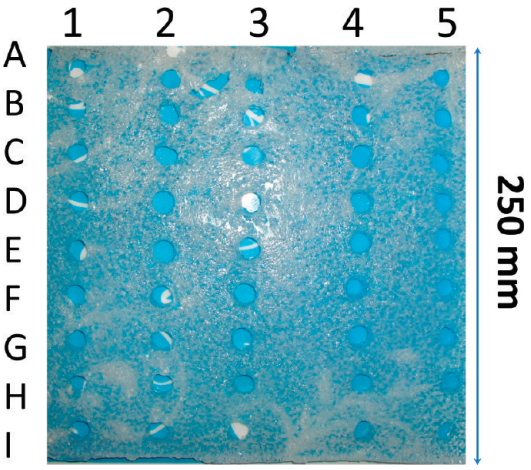


**Figure 6.** Matrix form of the sampling carried out after polymerization in the square reactor (300 × 300 × 15 mm$^3$).

Figure 7 shows the superposition of the molar mass distributions along the vertical axis 3A-3I (Figure 7a), the horizontal axis 1E-5E (Figure 7b) and the diagonal axis 1C-5G (Figure 7c). These superpositions show a reasonable homogeneity of the molar masses and distributions along all directions of the reactor. It should be noted that the ultrasound probe was terminated when the hot spot appeared in the IR-camera. When polymerization was carried out without terminating the ultrasound irradiation, the molar mass distribution showed chain degradation close to the probe, as expected.[55]

For each sample, the molar masses were raised by about a few millions ($\approx 3 \times 10^6$ g/mol; see peak of the molar masses $M_p$ in Figure 7), and the distribution curve presented a principal peak with a polydispersity index close to 1.6 and a trail toward the low molar masses due to the increase in temperature. Indeed, in the case of radical polymerization, the molar masses decreased with

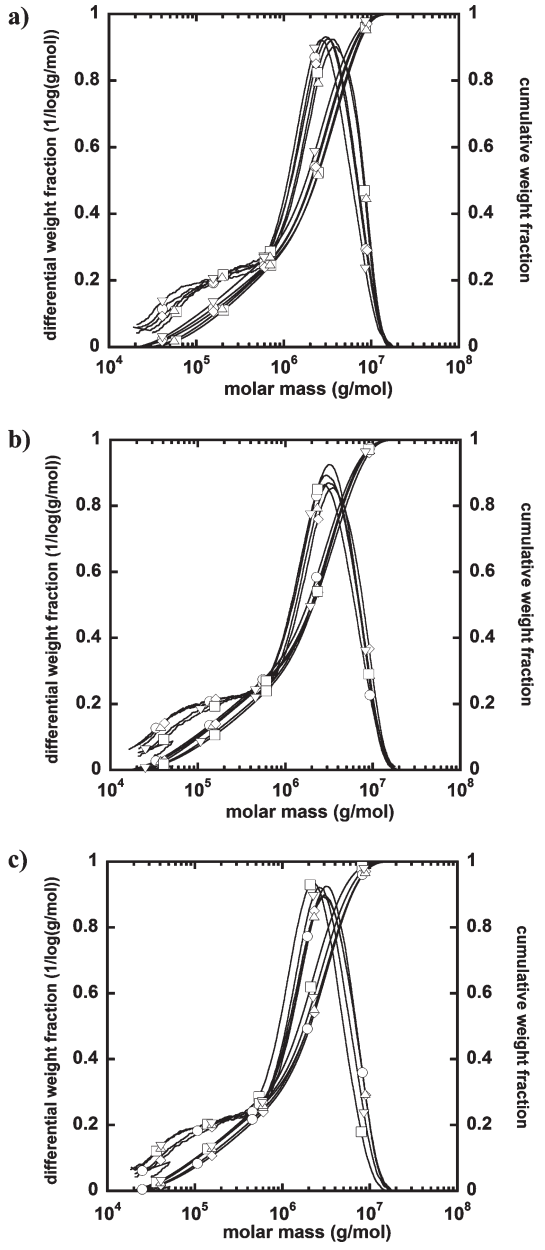


**Figure 7.** Superposition of the molar mass distributions along (a) the vertical axis 3A−3I (○, 3A; ◇, 3C; □, 3E; Δ, 3F; ▽, 3I), (b) the horizontal axis 1E-5E (○, 1E; ◇, 2E; □, 3E; Δ, 4E; ▽, 5E), and (c) the diagonal axis 1C-5G (○, 1C; ◇, 2D; □, 3E; Δ, 4F; ▽, 5G).

temperature which is a well-known characteristic of the radical polymerization of acrylamide.[54,56,57] The result is a strong polydispersity, with $I_p$ between 6 and 8, which is not that important for industrial applications. For model polyacrylamide with $I_p$ lower than 1.2, we invite the reader to consult prior reports on the nitroxide-mediated polymerization of acrylamide in gel processes.[4,5]

Knowing the increment of the refractive index and the UV responses of acrylamide and polyacrylamide in the SEC solvent, the residual monomer can be computed from the surface areas of the PAM and AM peaks by a method described in a previous work.[5] For all samples, the traces from the SEC experiments carried out on the reactive media displayed no acrylamide peak

**Table 1. Gel Process for Ultrasound-Assisted Polymerization of Acrylamide (35 wt %) in a Cylindrical Reactor (500 mL; Height = 200 mm; Diameter = 65 mm)**

| run | [AM]/[VAZO56] (wt %) | $T_{max}$ (°C) | $M_w$ ($10^6$ g/mol) |
|---|---|---|---|
| 1 | 1 | 100.4 | 1.3 |
| | | | 1.1 |
| | | | 1.2 |
| 2 | 1 | 99.7 | 1.2 |
| | | | 1.0 |
| | | | 1.3 |
| 3 | 1 | 100.2 | 1.1 |
| | | | 1.4 |
| | | | 1.5 |
| 4 | 0.1 | 102.8 | 2.1 |
| | | | 2.0 |
| | | | 2.2 |

according to both the RI and the UV detectors. On the basis of the precision of these two concentration detectors, it could thereby be assumed that the residual monomers were lower than 500 ppm.

This mode of thermal propagation is interesting in the context of gel processes because it shows that propagation can extend quickly in all directions of space in a classical cylindrical reactor. Polymerization assisted by ultrasound irradiation economizes reagents by reducing the number of chemical products necessary during the initiation of polymerization compared to classical redox initiator. As soon as polymerization has begun, the ultrasonic energy source is stopped and the exothermicity of the radical polymerization alone maintains polymerization until total polymer conversion without any particular risk because the temperature does not exceed 110 °C.

In addition, ultrasound-assisted polymerization was carried out in a classical cylindrical reactor with a large volume (500 mL; height, 200 mm; diameter, 65 mm) using the same acrylamide concentration (35 wt %) and the same ultrasound probe, which was plunged 20 mm into the surface. Front temperature measurements ($T_{max}$ = highest temperature) were recorded using a thermocouple plunged into the middle of the reactor. Each gel was sampled at the bottom, middle and top at its center for SEC analysis. The results are reported in Table 1. The residual monomer for all samples was lower than 500 ppm.

The molar mass distributions were similar to those obtained in the plane reactor, as described above (Figure 7). The results for runs no. 1, no. 2, and no. 3 demonstrate reasonable reproducibility, and run no. 4 illustrates the possibility of using a lower initiator concentration to obtain higher molar masses. Other experiments carried out with lower and higher acrylamide concentrations (20−40 wt %), copolymerization with 2-acrylamido-2-methyl-1-propanesulfonic acid sodium salt (AMPS) and sulfobetaine comonomers (5 and 20 mol %) and micellar copolymerization of acrylamide, AMPS, and hydrophobic monomers in the presence of SDS[46] have provided similar results. These results show that a gel process assisted by ultrasound irradiation allows the synthesis of a wide range of water-soluble polymers and associative polymers.[3] This gel process has some advantages over traditional methods of polymerization, including (1) short reaction times (a typical GP run takes only a few minutes, while classical polymerization techniques often require

a few hours); (2) low energy consumption (the low energy use is a consequence of applying the external energy source only in the first step, while in classical polymerization techniques, it is necessary for the full duration of the experiment); (3) maximization of atom economy (design syntheses limit the initiating product); and (4) its safety and ease of use. While green chemistry often seems to focus on industrial applications, it also applies to all other types of chemistry. GP improves process engineering, which is consistent with the goals of green chemistry.[58] The focus is on minimizing the hazard by 2D-IR thermography monitoring and on maximizing the efficiency of water-soluble polymer synthesis with ultrasound-assisted aqueous polymerization.

## 4. CONCLUSIONS

In this work, we have reported on the ultrasound-assisted radical polymerization of a water-soluble polymer via a gel polymerization process and a frontal polymerization method. The use of ultrasound not only suppresses the so-called "fingering" of frontal polymerization but also avoids any alteration of the molar mass distribution of the polymer. The ultrasound-assisted gel process has led to the formation of polymers with properties similar to those obtained by the classical polymerization routes, including conventional heating and low monomer concentration. We have shown by thought experiments and simulated approaches that 2D IR-thermography analysis makes it possible to demonstrate frontal polymerization in ultrasound-assisted GP and to monitor the front temperature and velocity. 2D-IR thermography monitoring of the gel polymerization process was used as a realistic approach for frontal polymerization analysis that occurs without a significant difference in the refractive index for the synthesized polymer versus the monomer/initiator mixture.

## ■ ASSOCIATED CONTENT

**Supporting Information.** Arrangement of the home-built plane reactor. This material is available free of charge via the Internet at http://pubs.acs.org.

## ■ ACKNOWLEDGMENT

The "Conseil Géneral d'Aquitaine" is gratefully acknowledged by J.R. for a Ph.D. grant, and the authors are grateful to the Thermal Engineering Department of the "IUT des Pays de l'Adour" for providing the IR Flir Thermacam system. The authors also thank Gérald Clisson for his technical assistance during the SEC experiments.

## ■ REFERENCES

(1) Williams, P. A. *Handbook of Industrial Water Soluble Polymers*; Blackwell Publishing Ltd.: Oxford, U.K.: 2007; p 332.
(2) Favero, C.; Gaillard, N. Improved process for enhanced oil recovery. WO2009044075 (A3), 2009.
(3) Zhu, Z. Y.; Jian, O. Y.; Paillet, S.; Desbrieres, J.; Grassl, B. *Eur. Polym. J.* **2007**, *43* (3), 824–834.
(4) Grassl, B.; Clisson, G.; Khoukh, A.; Billon, L. *Eur. Polym. J.* **2008**, *44* (1), 50–58.
(5) Rigolini, J.; Grassl, B.; Billon, L.; Reynaud, S.; Donard, O. F. X. *J. Polym. Sci., Part A: Polym. Chem.* **2009**, *47* (24), 6919–6931.
(6) Rigolini, J.; Grassl, B.; Reynaud, S.; Billon, L. *J. Polym. Sci., Part A: Polym. Chem.* **2010**, *48* (24), 5775–5782.
(7) Washington, R. P.; Steinbock, O. *J. Am. Chem. Soc.* **2001**, *123* (32), 7933–7934.
(8) Pojman, J. A.; Varisli, B.; Perryman, A.; Edwards, C.; Hoyle, C. *Macromolecules* **2004**, *37* (3), 691–693.
(9) Evstratova, S. I.; Antrim, D.; Fillingane, C.; Pojman, J. A. *J. Polym. Sci., Part A: Polym. Chem.* **2006**, *44* (11), 3601–3608.
(10) Fang, Y.; Yu, H.; Chen, L.; Chen, S. *Chem. Mater.* **2009**, *21* (19), 4711–4718.
(11) Alzari, V.; Monticelli, O.; Nuvoli, D.; Kenny, J. M.; Mariani, A. *Biomacromolecules* **2009**, *10* (9), 2672–2677.
(12) Yan, Q. Z.; Lu, G. D.; Zhang, W. F.; Ma, X. H.; Ge, C. C. *Adv. Funct. Mater.* **2007**, *17* (16), 3355–3362.
(13) Guo, X.; Wang, C. F.; Fang, Y.; Chen, L.; Chen, S. *J. Mater. Chem.* **2011**, *21* (4), 1124–1129.
(14) Tu, J.; Zhou, J.; Wang, C. F.; Zhang, O.; Chen, S. U. *J. Polym. Sci., Part A: Polym. Chem.* **2010**, *48* (18), 4005–4012.
(15) Scognamillo, S.; Alzari, V.; Nuvoli, D.; Mariani, A. *J. Polym. Sci., Part A: Polym. Chem.* **2010**, *48* (11), 2488–2490.
(16) Cintas, P.; Luche, J. L. *Green Chem.* **1999**, *1* (3), 115–125.
(17) Rocha, F. R. P.; Nobrega, J. A.; Fatibello, O. *Green Chem.* **2001**, *3* (5), 216–220.
(18) Chechilo, N. M.; Enikolopyan, Ns; Khvilivi, Ry *Dokl. Akad. Nauk SSSR* **1972**, *204* (5), 1180–&.
(19) Zhou, J.; Shao, H. A.; Tu, J.; Fang, Y. A.; Guo, X.; Wang, C. F.; Chen, L.; Chen, S. *Chem. Mater.* **2010**, *22* (19), 5653–5659.
(20) Tu, J.; Zhou, J.; Wang, C. F.; Zhang, Q. A.; Chen, S. *J. Polym. Sci., Part A: Polym. Chem.* **2010**, *48* (18), 4005–4012.
(21) Scognamillo, S.; Alzari, V.; Nuvoli, D.; Mariani, A. *J. Polym. Sci., Part A: Polym. Chem.* **2010**, *48* (11), 2486–2490.
(22) Davtyan, S. P.; Berlin, A. A.; Tonoyan, A. O. *Russ. Chem. Rev.* **2010**, *79* (3), 205–218.
(23) Fang, Y.; Chen, L.; Wang, C. F.; Chen, S. *J. Polym. Sci., Part A: Polym. Chem.* **2010**, *48* (10), 2170–2177.
(24) Tu, J.; Chen, L.; Fang, Y.; Wang, C.; Chen, S. *J. Polym. Sci., Part A: Polym. Chem.* **2010**, *48* (4), 823–831.
(25) Hayki, N.; Lecamp, L.; Desilles, N.; Lebaudy, P. *Macromolecules* **2010**, *43* (1), 177–184.
(26) Davtyan, S. P.; Zakaryan, H. H.; Tonoyan, A. O. *Chem. Eng. J.* **2009**, *155* (1−2), 292–297.
(27) Caria, G.; Alzari, V.; Monticelli, O.; Nuvoli, D.; Kenny, J. M.; Mariani, A. *J. Polym. Sci., Part A: Polym. Chem.* **2009**, *47* (5), 1422–1428.
(28) Mariani, A.; Nuvoli, D.; Alzari, V.; Pinf, M. *Macromolecules* **2008**, *41* (14), 5191–5196.
(29) Mariani, A.; Fiori, S.; Bidali, S.; Alzari, V.; Malucell, G. *J. Polym. Sci., Part A: Polym. Chem.* **2008**, *46* (10), 3344–3352.
(30) Jimenez, Z.; Pojman, J. A. *J. Polym. Sci., Part A: Polym. Chem.* **2007**, *45* (13), 2745–2754.
(31) Crivello, J. V. *J. Polym. Sci., Part A: Polym. Chem.* **2006**, *44* (21), 6435–6448.
(32) Chen, S.; Tian, Y.; Chen, L.; Hu, T. *Chem. Mater.* **2006**, *18* (8), 2159–2163.
(33) Nason, C.; Roper, T.; Hoyle, C.; Pojman, J. A. *Macromolecules* **2005**, *38* (13), 5506–5512.
(34) Chen, S.; Sui, J. J.; Chen, L.; Pojman, J. A. *J. Polym. Sci., Part A: Polym. Chem.* **2005**, *43* (8), 1670–1680.
(35) Crivello, J. V.; Falk, R.; Zonca, M. R. *J. Polym. Sci., Part A: Polym. Chem.* **2004**, *42* (7), 1630–1646.
(36) Mariani, A.; Bidali, S.; Fiori, S.; Sangermano, M.; Malucelli, G.; Bongiovann, R.; Priola, A. *J. Polym. Sci., Part A: Polym. Chem.* **2004**, *42* (9), 2066–2072.
(37) Fiori, S.; Mariani, A.; Ricco, L.; Russo, S. *Macromolecules* **2003**, *36* (8), 2674–2679.
(38) Gill, N.; Pojman, J. A.; Willis, J.; Whitehead, J. B. *J. Polym. Sci., Part A: Polym. Chem.* **2003**, *41* (1), 204–212.
(39) Mariani, A.; Fiori, S.; Chekanov, Y.; Pojman, J. A. *Macromolecules* **2001**, *34* (19), 6539–6541.
(40) Fortenberry, D. I.; Pojman, J. A. *J. Polym. Sci., Part A: Polym. Chem.* **2000**, *38* (7), 1129–1135.

(41) Chekanov, Y. A.; Pojman, J. A. *J. Appl. Polym. Sci.* **2000**, *78* (13), 2398–2404.
(42) Pojman, J. A.; Elcan, W.; Khan, A. M.; Mathias, L. *J. Polym. Sci., Part A: Polym. Chem.* **1997**, *35* (2), 227–230.
(43) Pojman, J. A.; Ilyashenko, V. M.; Khan, A. M. *J. Chem. Soc., Faraday Trans.* **1996**, *92* (16), 2825–2837.
(44) Khan, A. M.; Pojman, J. A. *Trends Polym. Sci.* **1996**, *4* (8), 253–257.
(45) Pojman, J. A.; Curtis, G.; Ilyashenko, V. M. *J. Am. Chem. Soc.* **1996**, *118* (15), 3783–3784.
(46) Dupuis, G.; Rigolini, J.; Clisson, G.; Rousseau, D.; Tabary, R.; Grassl, B. *Anal. Chem.* **2009**, *81* (21), 8993–9001.
(47) Christie, D. I.; Gilbert, R. G.; Congalidis, J. P.; Richards, J. R.; McMinn, J. H. *Macromolecules* **2001**, *34* (15), 5158–5168.
(48) Alam, M. N.; Zetterlund, P. B.; Okubo, M. *Polymer* **2008**, *49* (4), 883–892.
(49) El Omari, K.; Le Guer, Y. *Int. J. Heat Mass Transfer* **2010**, *53* (1−3), 123–134.
(50) Pojman, J. A.; Viner, V.; Binici, B.; Lavergne, S.; Winsper, M.; Golovaty, D.; Gross, L. *Chaos* **2007**, *17*, 3.
(51) Pojman, J. A.; Masere, J.; Petretto, E.; Rustici, M.; Huh, D. S.; Kim, M. S.; Volpert, V. *Chaos* **2002**, *12* (1), 56–65.
(52) Masere, J.; Stewart, F.; Meehan, T.; Pojman, J. A. *Chaos* **1999**, *9* (2), 315–322.
(53) Ilyashenko, V. M.; Pojman, J. A. *Chaos* **1998**, *8* (1), 285–289.
(54) Giz, A.; Catalgil-Giz, H.; Alb, A.; Brousseau, J. L.; Reed, W. F. *Macromolecules* **2001**, *34* (5), 1180–1191.
(55) Vijayalakshmi, S. P.; Madras, G. *Polym. Degrad. Stab.* **2005**, *90* (1), 116–122.
(56) Grassl, B.; Alb, A. M.; Reed, W. F. *Macromol. Chem. Phys.* **2001**, *202* (12), 2518–2524.
(57) Grassl, B.; Reed, W. F. *Macromol. Chem. Phys.* **2002**, *203* (3), 586–597.
(58) Anastas, P. T.; Kirchhoff, M. M. *Acc. Chem. Res.* **2002**, *35* (9), 686–694.